Construction of Sr@Mn_3O_4/GO Nanocomposite: A Synergistic Electrocatalyst for Nitrofurantoin Detection in Biological and Environmental Samples

Venkatachalam Vinothkumar[a,b,c†], Rajalakshmi Sakthivel[c†], Shen-Ming Chen[c], Arumugam Sangili[c], Tae Hyun Kim[a,b]**

[a]*Department of Chemistry, Soonchunhyang University, Asan 31538, Republic of Korea*

[b]*Department of ICT Environmental Health System, Graduate School, Soonchunhyang University, Asan 31538, Republic of Korea*

[c]*Department of Chemical Engineering and Biotechnology, College of Engineering, National Taipei University of Technology, No. 1, Section 3, Chung-Hsiao East Road, Taipei 10608, Taiwan, ROC*

Corresponding Authors:

Prof. Shen-Ming Chen (E-mail: smchen78@ms15.hinet.net).

Prof. Tae Hyun Kim (E-mail: thkim@sch.ac.kr).

†These authors contributed equally

Number of pages: 09

Number of figures: 10

S1. Chemicals

Strontium chloride hexahydrate ($SrCl_2 \cdot 6H_2O$, ≥99%), manganese chloride tetrahydrate ($MnCl_2 \cdot 4H_2O$, 99.99%), nitrofurantoin ($C_8H_6N_4O_5$, 98.0–102.0%), graphite (99.99%), potassium permanganate ($KMnO_4$, >99%), sodium nitrate ($NaNO_3$, >99%), liquid ammonia solution (Liq. NH_3, 25 wt%), disodium hydrogen phosphate (Na_2HPO_4), hydrochloric acid (HCl), sulfuric acid (H_2SO_4, 99.99%), and monosodium dihydrogen orthophosphate (NaH_2PO_4) were purchased in the Sigma Aldrich (United States). 0.1 M phosphate buffer (PB) was prepared by dissolving Na_2HPO_4 and NaH_2PO_4 in Millipore water and it neutralizing with 0.1 M HCl /or NaOH. Millipore water (18.25 MΩ cm^{-1}) was used to prepare all the solutions.

S2. Characterization techniques

The crystalline structure of the as-proposed materials was discovered by X-ray diffraction (XRD) using a PANalytical X'PERT PRO diffractometer (EMPYREAN, Malvern Panalytical, The Netherlands) with Cu Kα radiation = 1.5417 Å. Using the JASCO 4600LE Shimadzu (Japan), Fourier transform infrared (FT-IR) spectra in the 4000–400 cm^{-1} region were measured. The Raman spectrum was studied with UniNanoTech, ACRON (South Korea). The surface area of the as-synthesized samples was investigated using the Brunauer-Emmett-Teller (BET; ASAP 2020, Micromeritics, USA) isotherm. Thermo Scientific Multi-Lab 2000 (Thermo Fisher Scientific/United States) X-ray photoelectron microscopy (XPS) was used to demonstrate the Sr, Mn, O, and C molecules in the Sr@Mn_3O_4/GO nanocomposite. Surface morphologies of Mn_3O_4, Sr@Mn_3O_4, GO, and Sr@Mn_3O_4/GO were explored via field emission scanning electron microscopy (FESEM/JEOL-JSM-6500F) and transmission electron microscopy (TEM)/JEOL-JEM-2100F) (JEOL Ltd./United States) instruments, as well as energy dispersive X-ray (EDX) and mapping studies.

S3. Electrochemical methods

The electrochemical performance of the resultant nanocomposite was explored through electrochemical impedance spectroscopy (EIS), cyclic voltammetry (CV), and differential pulse voltammetry (DPV) using the XPot–ZAHNER–Elektrik, and CHI 410A techniques. EIS measurements were applied to the frequency ranges of 0.1 Hz to 10^5 kHz with the potential of 5 mV in 0.1 M KCl/5 mM $[Fe(CN)_6]^{3-/4-}$ solution. The electrochemical (CV and DPV) experiments were carried out using a conventional three-electrode system with a glassy carbon electrode (GCE), Ag/AgCl-saturated KCl electrode, and Pt wire corresponding to the working (diameter of 0.07 cm^2), reference, and counter electrodes, respectively. DPV parameters were used in the following order: pulse width = 50 ms, pulse amplitude = 50 mV, step potential = 0.004 V, scan rate = 50 mV s^{-1}, modulation time = 2 s, and interval time = 0.2 s.

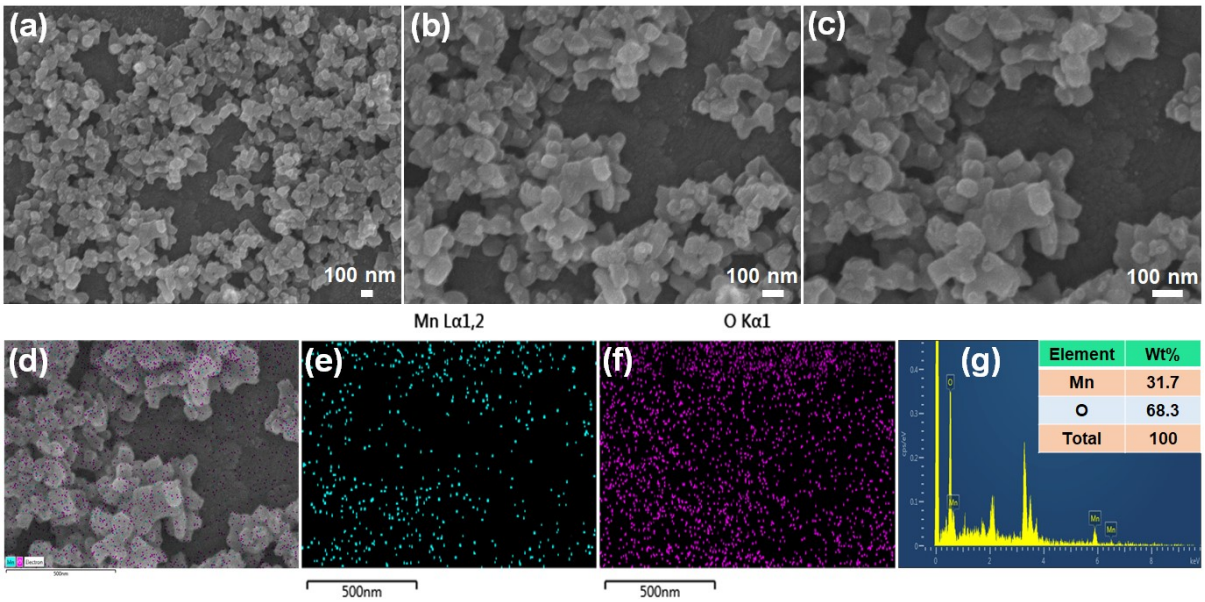

Fig. S1. FESEM images of Mn_3O_4 at different magnifications (a–c). Elemental mapping of Mn_3O_4–Mix (d), Mn (e), and O (f). EDX analysis of Mn_3O_4 with their weight percentage (g).

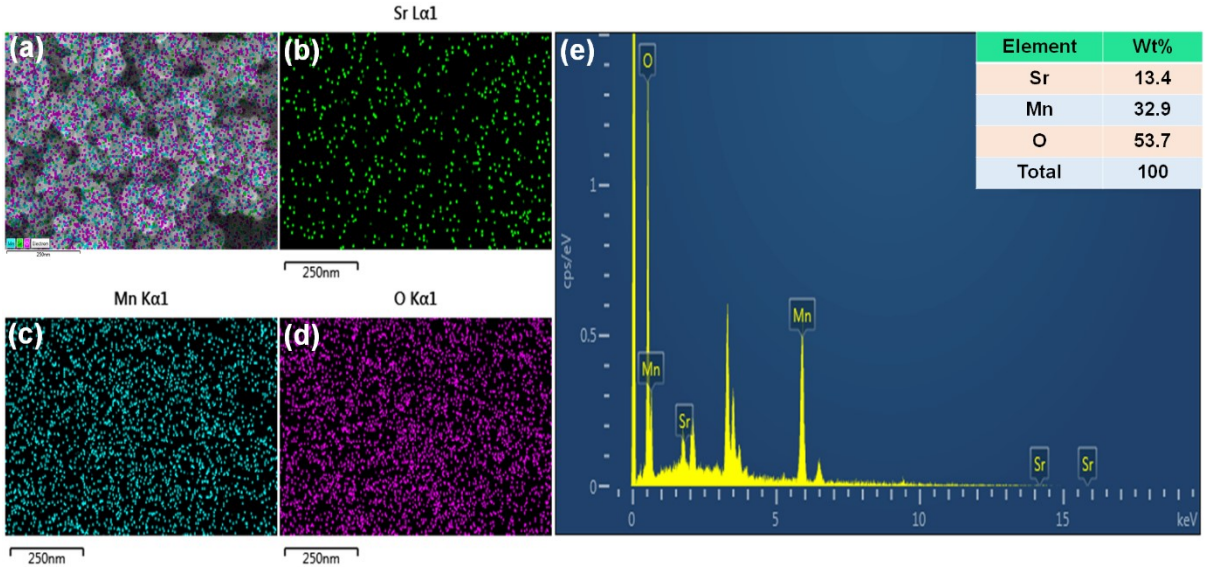

Fig. S2. Elemental mapping of Sr@Mn_3O_4–Mix (a), Sr (b), Mn (c), and O (d), and EDX analysis of Sr@Mn_3O_4 with their weight percentage (e).

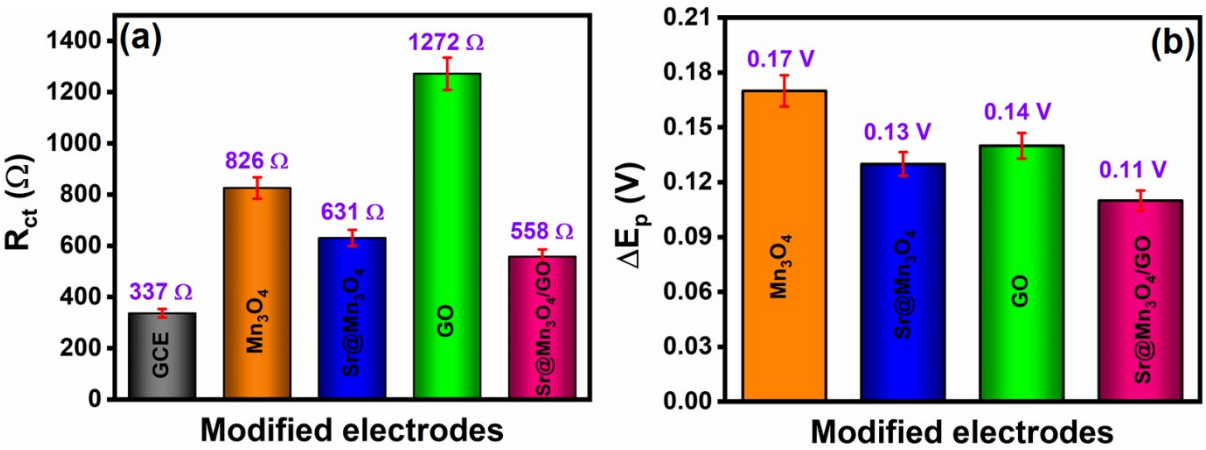

Fig. S3. Bar chart of different modified electrodes with corresponding R_{ct} values (a). Bar graph of various modified electrodes with the peak-to-peak separation (ΔE_p) values (b).

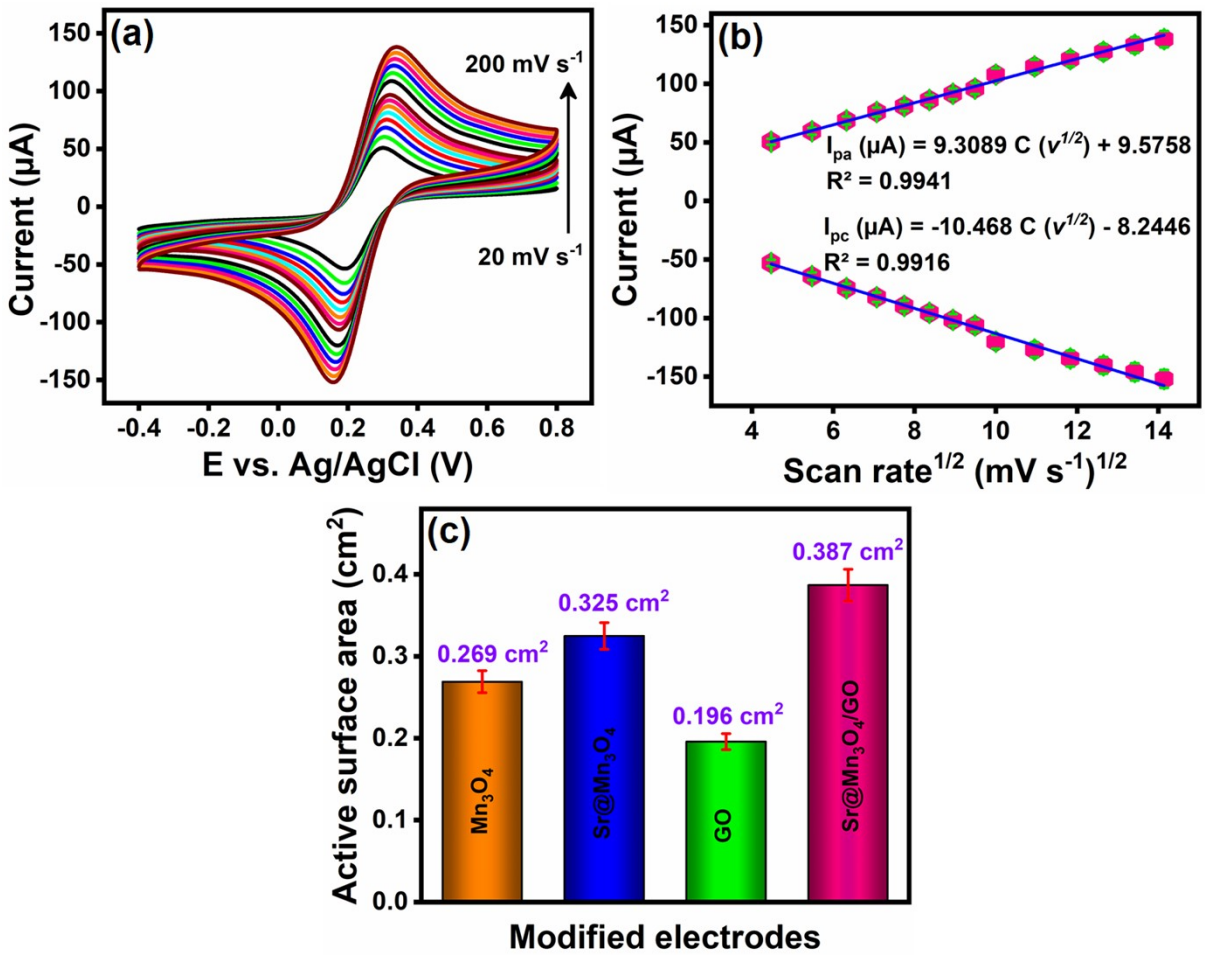

Fig. S4. CV curves of diverse scan rates (20 to 200 mV s^{-1}) on Sr@Mn_3O_4/GO/GCE (a) and the corresponding linear plot (b). Bar graph of diversely modified electrodes with the related active surface area (c).

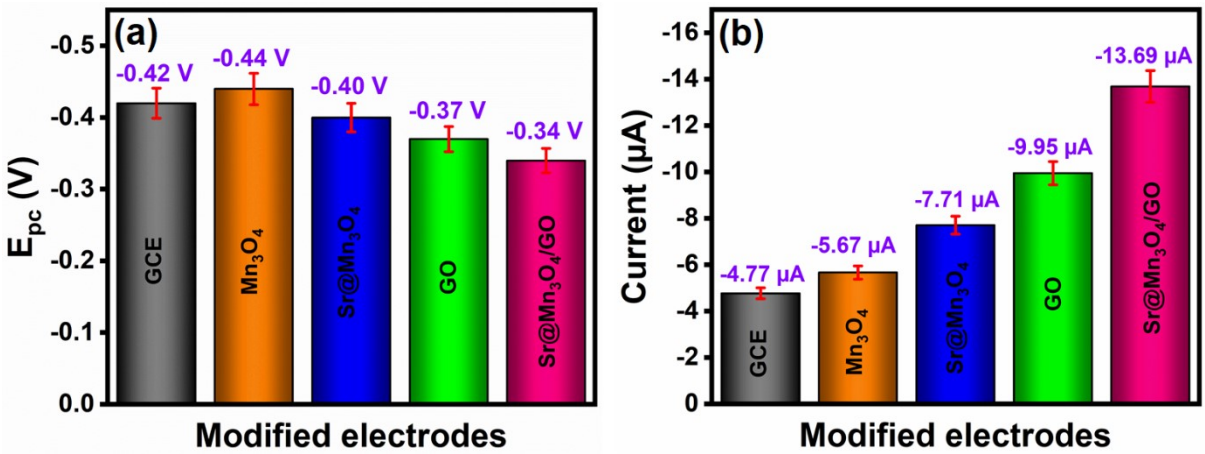

Fig. S5. Bar chart of different modified electrodes with their E_{pc} (a), and (b) I_{pc} values.

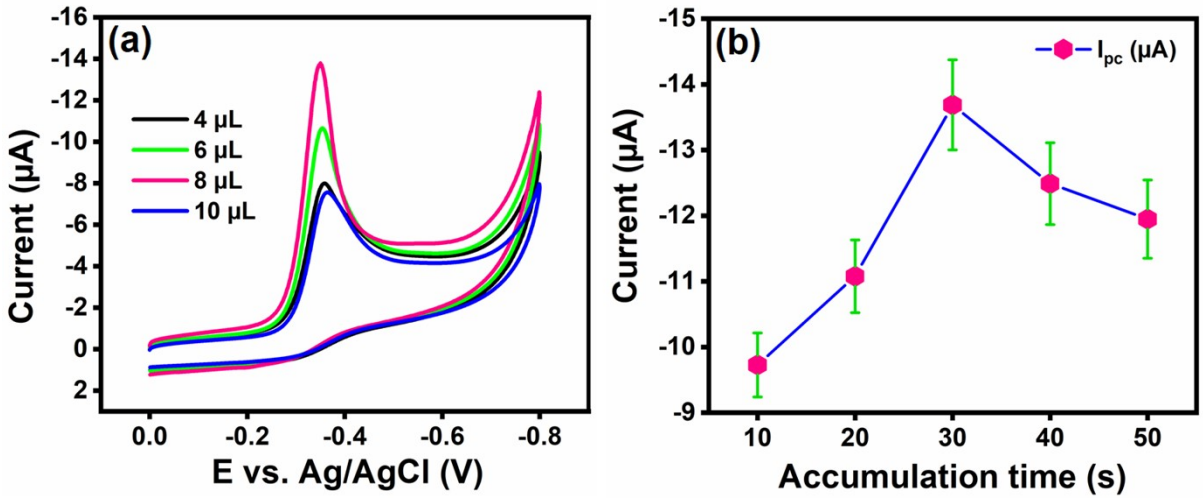

Fig. S6. CV curves of diverse loading amounts (4 to 10 μL) of Sr@Mn_3O_4/GO/GCE (a), and the plot for accumulation times versus I_{pc} (b) for NFT detection.

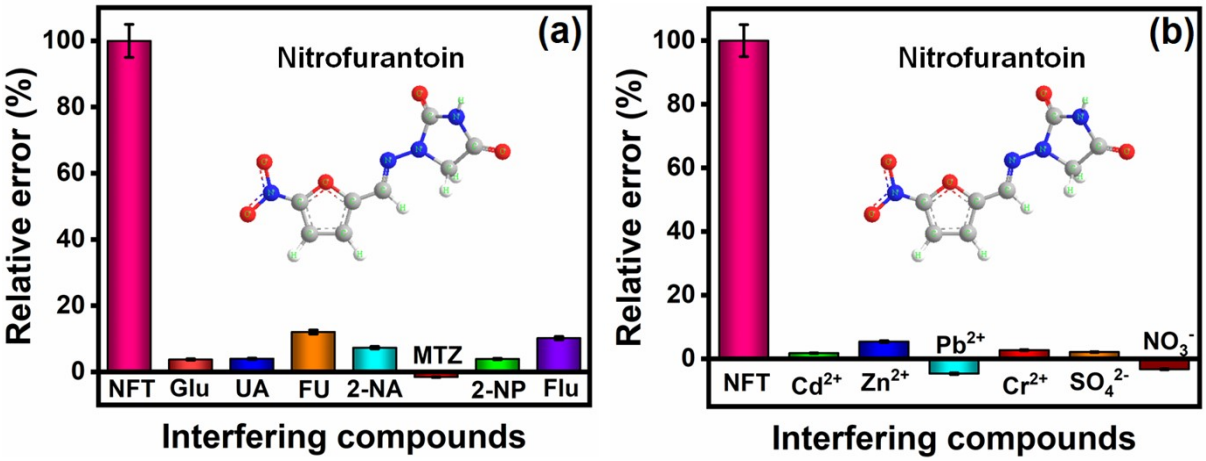

Fig. S7. Bar chart of NFT with different biomolecules and potential interfering nitro compounds with the corresponding relative error (%) (a), and NFT with inorganic metal ions with the related error (%) (b).

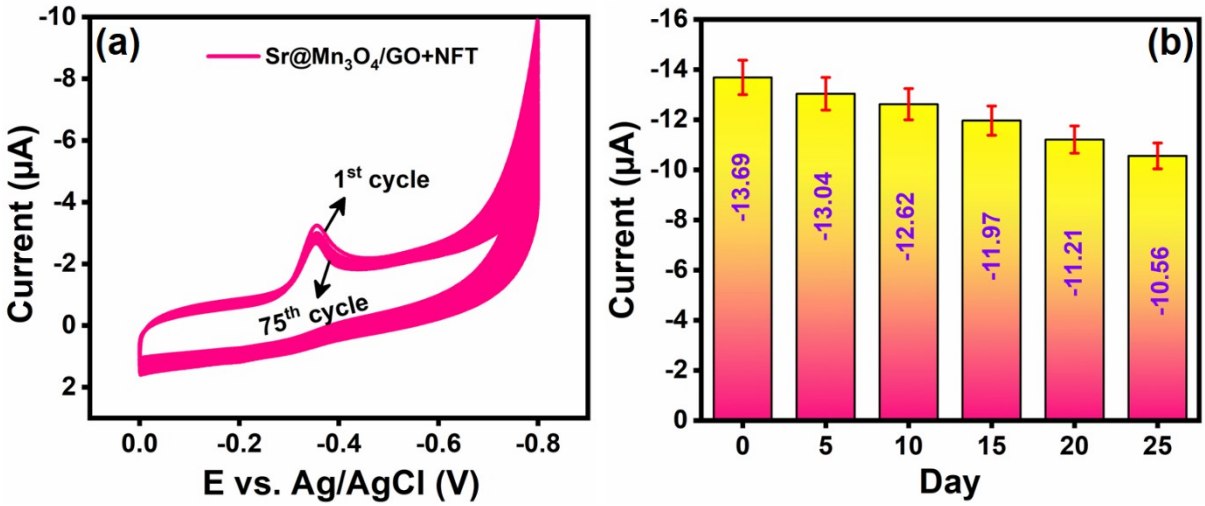

Fig. S8. CV response for Sr@Mn_3O_4/GO/GCE in the cyclic stability test (75 cycles) (a), and bar chart of storage stability (for 0 to 25 days) with their I_{pc} (b).

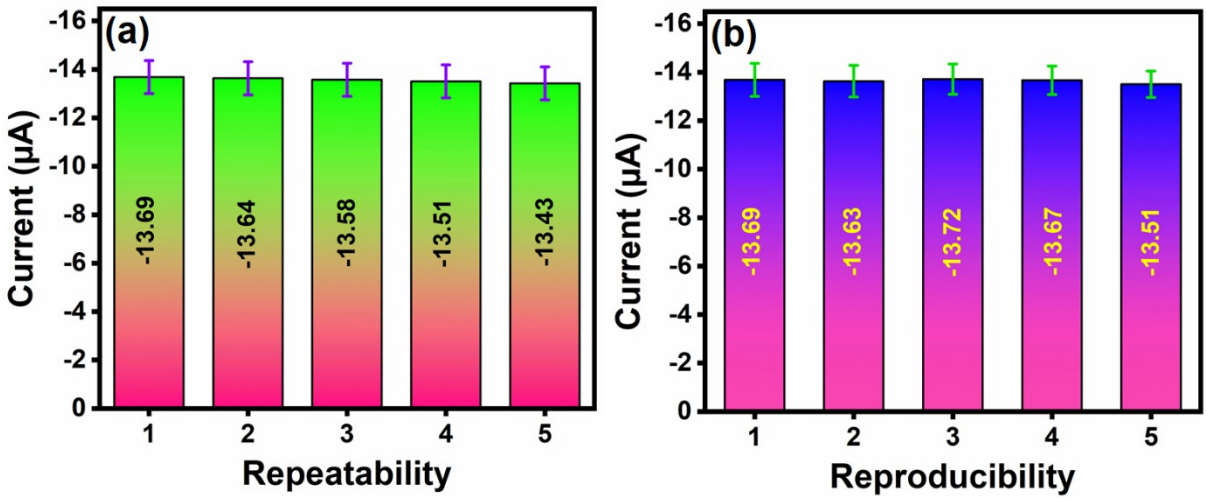

Fig. S9. Repeatability (a), and reproducibility (b) of Sr@Mn_3O_4/GO/GCE for NFT reduction.

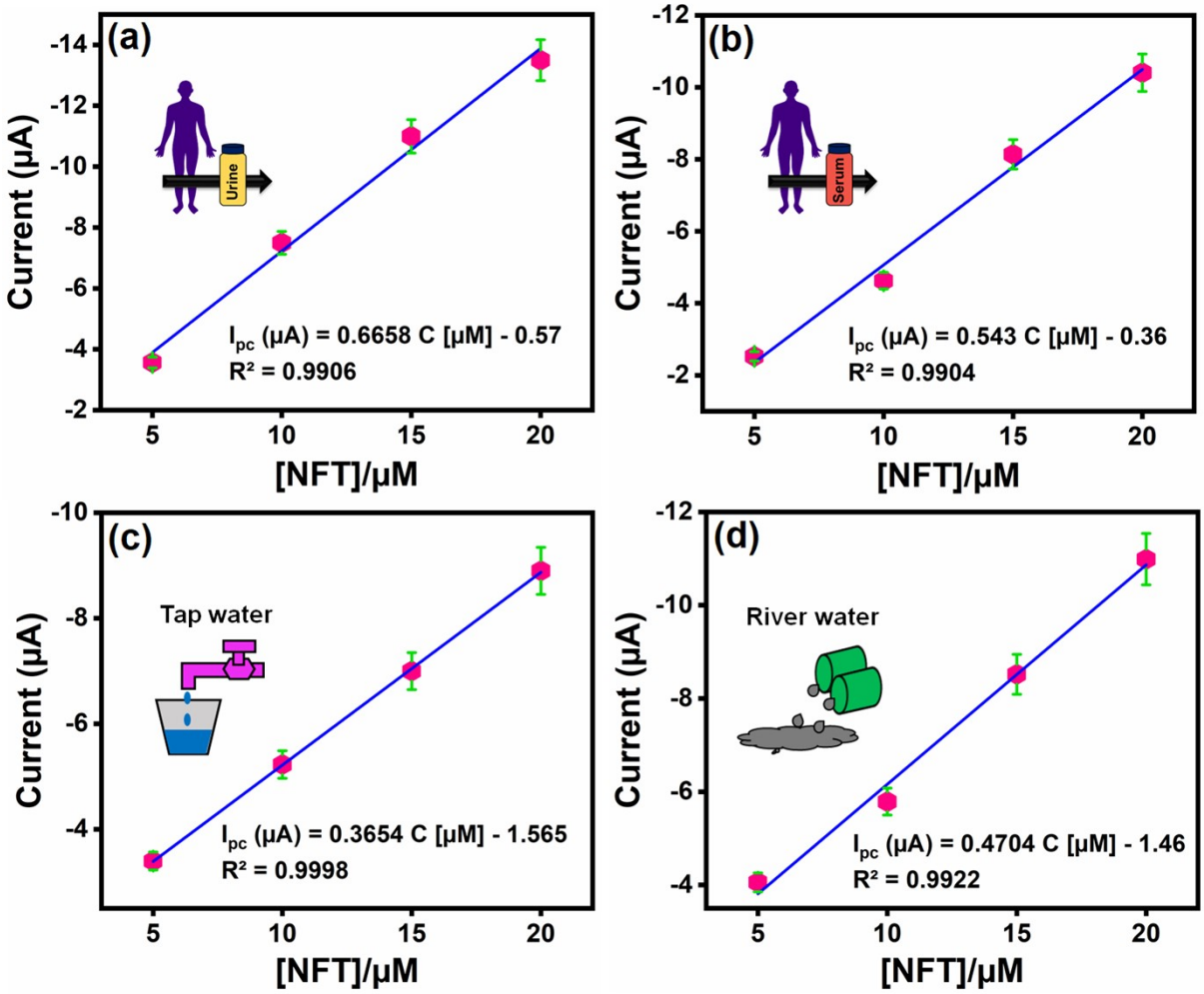

Fig. S10. The linear graph between I_{pc} and NFT concentrations of the human urine, human serum, tap water, and river water samples (a–d).